BUCKLING STRENGTH OF GFRP EQUAL-LEG ANGLE STRUCTURAL MEMBERS UNDER CONCENTRIC AXIAL COMPRESSION

Sittichai Seangatith[1*]

Abstract

This paper presents the results of a study on the buckling strength of glass fiber-reinforced plastic (GFRP) equal-leg angle structural members subjected to the concentric axial compression. The angle members were made of glass fiber reinforced with polyester resin and manufactured by a pultrusion process. A total of 32 specimens with slenderness ratios ranging from 12 to 187 and leg width-to-thickness ratios of 8, 12, and 16 were tested. The experimentally obtained buckling loads were also predicted by using analytical formulas. The analytical formulas were developed by modifying a well-known elastic flexural-torsional buckling theory with some factors concerning the orthotropic behaviors of the GFRP material. Coupons cut from the angle specimens were tested using compression and in-plane shear coupon test to determine necessary material properties. The analytical results were then correlated to the test results and those calculated by the nominal buckling strength equations proposed by Zureick and Steffen to validate the adequacy. Finally, the design equations for the angle members were proposed.

Keywords: Glass fiber reinforced plastic, GFRP, angle member, axial compression, flexural buckling, flexural-torsional buckling, buckling strength

Introduction

Glass fiber-reinforced plastic (GFRP) composite has emerged as an effective material for civil engineering structures for over 20 years (Ballinger, 1990). The GFRP material has superior characteristics in corrosion resistance, strength-to-weight ratio, and ease of handling in construction over the conventional materials such as steel and reinforced concrete. Many American, European, and international industries are currently producing a variety of GFRP structural sections such as I, W, angle, channel, and box. Among various types of manufacturing processes that have evolved during the past four decades, the pultrusion process appears to offer the highest productivity-to-cost ratio (Zureick and Scott, 1997). This is because it allows a mass production of long, straight, and constant structural sections. While the GFRP structural sections become readily available, designers of such components are facing an immediate problem in the lack of reliable design criteria. Thus, there is an urgent need to understand the behavior and strength of the GFRP structures and their components under various types of loading condition.

[1] *School of Civil Engineering, Institute of Engineering, Suranaree University of Technology, Nakhon Ratchasima 30000, Thailand*

[*] *Corresponding author*

During the past few years, extensive research works have been performed on the fiber-reinforced plastic (FRP) structural members subjected to the axial compression with different kinds of cross-section (Lee and Hewson 1978; Mottram 1991; Barbero and Raftoyiannis 1993; Yuan and Seangatith 1996; Yuan 1997; Zureick and Scott 1997; Seangatith and Sriboonlue 1999). Most of these studies have concentrated on the flexural buckling behavior of the members having doubly symmetric cross-sections such as box-, I-, and W-sections. The GFRP angles are commonly used in a variety of structures and structural components such as trusses, frames, and bracing members because they can be easily fabricated and erected. They, however, have not received the same degree of attention as the other sections. Only few works have been reported on the study on the behavior and design of the axially loaded GFRP equal-leg angle members (Zureick and Steffen, 2000). In addition, the design process of these kinds of structural member under either the concentric or the eccentric axial loads requires the knowledge of concentrically compressive load capacity of the member. This paper presents the results of a study on the behavior and buckling strength of the GFRP equal-leg angle structural members under the concentric axial compression. The analytical formulas were developed from a well-known elastic flexural-torsional buckling theory, incorporating some factors associated with the orthotropic behaviors of the GFRP material. Correlation studies between the test results and those from the analytical formulas and the nominal buckling strength equations proposed in Zureick and Steffen (2000) were conducted. The effects of effective-length factors and material orthotropy on the buckling strength were investigated. Finally, the design equations are presented.

Previous Research Works

ASCE has issued a structural plastic design manual (ASCE structural plastic design manual, 1984) which was intended to be a guideline for engineers who work with structural plastics. The manual recommends that the buckling resistance of single angle member subjected to axially compressive load can be approximated by the lower value determined from the flexural buckling and torsional buckling equations. For the members failing in flexural buckling, the flexural buckling strength, $\sigma_{xc,\mathrm{Fl}}$, can be calculated from Euler's flexural buckling equation:

$$\sigma_{xc,\mathrm{Fl}} = \frac{\pi^2 E}{\left(KL/r\right)^2} \tag{1}$$

where E is the modulus of elasticity for bending in the direction of buckling, L is the length, K is the effective-length factor, and r is the radius of gyration in that direction. For the members failing in torsional buckling, the torsional buckling strength, $\sigma_{xc,\mathrm{T}}$, can be estimated from the torsional buckling equation for a linearly elastic isotropic materials:

$$\sigma_{xc,\mathrm{T}} = \frac{E_L}{2(1+v_{LT})}\left(\frac{t}{b}\right)^2 \tag{2}$$

where E_L is the longitudinal compression modulus, v_{TL} is the major Poisson's ratio, and t and b are the leg thickness and the leg width of the section, respectively. It is well known that the value of the term $E_L/[2(1+v_{LT})]$ for GFRP is always greater than that of the in-plane shear modulus, G_{LT}, by over two times (Seangatith, 1999). Thus, Eqn. (2) always overestimates the torsional buckling strength of the GFRP structural members. For the members failing in flexural-torsional buckling, the buckling strength can be approximated by using an interaction relationship between the flexural and torsional buckling strength equations. A few forms of the relationship are proposed, but is not specified, being left to the judgement of the designer.

Zureick and Steffen (2000) presented the results of a study on the short term behavior of concentrically loaded single angle members, made of pultruded glass fiber-reinforced polymeric materials. A total of 25 specimens were tested with KL/r ratios ranging from 30 to 105 and b/t ratios of 8, 10.7, 12, 16, and 24. Under axial compression, the GFRP angle members buckle in either flexural or flexural-

torsional mode. Analytical equations that describe the buckling behavior of specially orthotropic, centrally loaded, equal-leg angle section were derived. The compression and in-plane shear coupon tests of the material from each specimen were also conducted. The results were statistically analyzed to obtain the 95% lower confidence limit on the fifth percentile strength and modulus values. These material properties were used in the analytical buckling equations to correlate the test results to the analytical results in order to obtain the design strength, ϕP_n, of the angle members. It is proposed that the nominal strength, P_n, of the members, can be taken as the lowest value determined in accordance with the limit states of the flexural buckling, the flexural-torsional buckling, and the material compression strength. For the limit state of the flexural buckling, the nominal buckling load is determined by using the equation

$$P_n = \frac{\pi^2 E_L}{(KL/r)^2} A_g \qquad (3)$$

where E_L is the longitudinal compressive modulus of elasticity and A_g is the gross cross-sectional area of the member. It should be noted that Eqn. (3) is similar to Eqn. (1), except that E is replaced by E_L. For the limit state of the flexural-torsional buckling, the nominal buckling load is determined by using the equation

$$P_n = 0.9 \frac{G_{LT}}{(b/t)^2} A_g \qquad (4)$$

Eqn. (4) is similar to Eqn. (2), except that the term $E/[2(1 + v)]$ is replaced by the in-plane shear modulus, G_{LT}, obtained experimentally from the in-plane shear coupon test, and the factor of 0.9 was proposed based on the approximation that the flexural-torsional buckling load is approximately equal to 90% of the torsional buckling. For the limit state of the material compressive failure, the nominal strength is determined by

$$P_n = \sigma_L^c A_g \qquad (5)$$

where σ_L^c is the ultimate longitudinal compressive strength of the GFRP material. By using Monte Carlo simulation, the resistance

factor, ϕ, was proposed as follows: $\phi = 0.65$ for the flexural buckling limit state; for the flexural-torsional buckling limit state; and for the material compressive limit state. It can be seen that Eqns. (3) and (4) are a better-developed form of Eqns. (1) and (2), respectively.

It is well-known that a number of design equations for the concentrically loaded GFRP equal-leg angle members have been proposed by the GFRP manufacturers. Most of these equations are practical and easy to use. They have been developed based on full-scale test results of the structural members and curve-fitting. These equations are, however, recommended to be used only for their products.

From the review of the previous research works, it is believed that the buckling strength equations of the GFRP equal-leg angle structural member subjected to the concentric axial compression can be derived in a well-developed form without introducing any curve-fit-based coefficients or flexural-torsional buckling related factors. In addition, since the GFRP material has a high E_L/G_{LT} ratio or high orthotropy, which is usually in the range of two to four times as high as that of the steel (Zureick and Scott 1997; Seangatith, 1999; Mottram 2004), it exhibits a larger effect from shear deformation when compared with that of the isotropic material. Therefore, the effect of the transverse shear should be included into the buckling stress equations, and hence a more realistic behavior of the structural member can be determined.

Analytical Formulas

A concentrically loaded equal-leg angle structural member can fail in by flexural or flexural-torsional buckling. Trahair (1993) showed that if the angle member is perfectly straight and is subjected to only the concentrically axial force, the resistance to buckling depends on its resistance to bending and torsion. The lowest buckling resistance of the member will govern the buckling mode. In this development, the GFRP material is assumed to be a specially orthotropic homogeneous material that can be characterized by using four independent elastic constants: the longitudinal

compressive modulus of elasticity, E_L, the in-plane shear modulus, G_{LT}, the major Poisson's ratio, v_{LT}, and the transverse modulus of elasticity, E_T

Figure 1 shows a typical configuration of an equal-leg angle cross-section in a fixed Cartesian coordinate system (x', y', z') in which the principal $x'-$ and $y'-$axes lie in the plane of the cross-section and z'-axis the coincides with the longitudinal z'-axis of the angle member. Point C is the centroid and point S is the shear center of the cross-section. Each leg has the width of b and the thickness of t. Following the analysis developed by Trahair for the case of the GFRP equal-leg angle member subjected to concentric axial load, P, the differential equations which describe the equilibrium in its buckled configuration, i.e. displaced laterally u in $x'-$axis and v in $y'-$axes and twisted by φ in $x'-y'$ plane may be rewritten as

$$\left(E_L I_{x'}(v'')\right)'' = -\left(P(v')\right)' + \left(Px_o'(\varphi)'\right)' \quad (6)$$

$$\left(E_L I_{y'}(u'')\right)'' = -\left(P(u')\right)' \quad (7)$$

$$\left(E_L C_w(\varphi)''\right)'' - \left(G_{LT}J(\varphi)'\right)' = \quad (8)$$
$$- \left(P\, r_2^2(\varphi)'\right)' + \left(Px_o'(v)'\right)'$$

where $(\ )'$ denotes the differential operator $d(\ )/dz'$, $I_{x'}$ and $I_{y'}$ are the moment of inertia of the cross-sectional area about $x'-$and $y'-$axes, respectively, J is the polar moment of inertia, $r_2^2 = \dfrac{I_{x'} + I_{y'}}{A} + x_o'^2$, and C_w is the warping constant. For the equal-leg angle, $C_w = A^3/144$.

For angle member with simply supported boundary conditions (contrained rotation about the z'-axis and free to warp) at the coordinate $z' = 0$ and $z' = L$, the boundary conditions are

$$u(0) = u(L) = v(0) = v(L) = \varphi(0) = \varphi(L) = 0 \quad (9)$$

$$u''(0) = u''(L) = v''(0) = v''(L) = \varphi''(0) = \varphi''(L) = 0 \quad (10)$$

Eqns. (6) to (10) can be satisfied by the buckled shapes, $\dfrac{u}{\delta_{x'}} = \dfrac{v}{\delta_{y'}} = \dfrac{\varphi}{\theta} = \sin\dfrac{\pi z}{L}$, if the

axial force satisfies the following determinant

$$\begin{vmatrix} (P_{x'} - P) & 0 & Px_o' \\ 0 & (P_{y'} - P) & 0 \\ Px_o' & 0 & r_2^2(P_{z'} - P) \end{vmatrix} = 0 \quad (11)$$

Expanding the determinant, Eqn. (11) can be rewritten as

$$f(P) = P^3[r_2^2 - x_o'^2] - P^2[(P_{x'} + P_{y'} + P_{z'})r_2^2 -$$
$$P_y x_o'^2] + Pr_2^2[(P_{x'}P_{y'} + P_{y'}P_{z'} + P_{z'}P_{x'}]$$
$$- P_{x'}P_{y'}P_{z'}r_2^2 = 0 \quad (12)$$

Rearranging Eqn. (12),

$$(P_{y'} - P)[r_2^2(P_{x'} - P)(P_{z'} - P) - (Px_o')^2] = 0 \quad (13)$$

The solutions of Eqn. (13) are

$$P_1 = P_{y'} \quad (14.a)$$

$$P_2 = \frac{(P_{x'} + P_{z'}) + \sqrt{(P_{x'} + P_{z'})^2 - 4P_{x'}P_{z'}r_o^2/r_2^2}}{2r_o^2/r_2^2} \quad (14.b)$$

$$P_3 = \frac{(P_{x'} + P_{z'}) - \sqrt{(P_{x'} + P_{z'})^2 - 4P_{x'}P_{z'}r_o^2/r_2^2}}{2r_o^2/r_2^2} \quad (14.c)$$
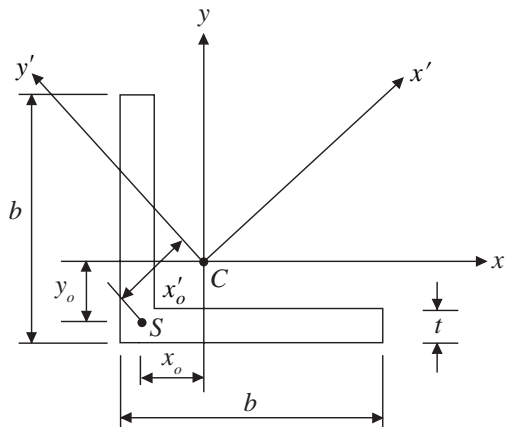

Figure 1. Typical configuration of equal-leg angle cross-section.

where $r_o^2 = \dfrac{I_{x'} + I_{y'}}{A_g}$. $P_{x'}, P_{y'}$, and $P_{z'}$ are the flexural buckling load about x'-axis, the flexural buckling load about y'-axis, and the torsional buckling load about z'-axis, respectively.

Since the GFRP material has a high orthotropy or high E_L / G_{LT} ratio, the effect of the shear on the flexural buckling load may need to be considered. In addition, it should be noted that, for the equal-leg angle with different end-restrained conditions, the lengths for bending and twisting may be assumed as the distances between the inflection points of the buckled shapes. Lee and Hewson (1978) suggested that the flexural buckling load about x'-axis and y'-axis of the FRP structural member should be estimated by using the equations:

$$P_{x'} = \frac{\pi^2 E_L I_{x'}}{L_{x'}^2}\left[\frac{1}{1 + n\pi^2 E_L I_{x'} / L_{x'}^2 A_g G_{LT}}\right] \quad (15)$$

$$P_{y'} = \frac{\pi^2 E_L I_{y'}}{L_{y'}^2}\left[\frac{1}{1 + n\pi^2 E_L I_{y'} / L_{y'}^2 A_g G_{LT}}\right] \quad (16)$$

where $K_{x'} L_{x'}$ and $K_{y'} L_{y'}$ are effective lengths for bending about the principal axis x' and y', respectively and n is the form factor which is assumed to be 2 and 3 for the flexural buckling about x'- and y'-axes, respectively (Lee and Hewson, 1978). The torsional buckling load can be calculated by using the equation:

$$P_{z'} = \frac{G_{LT} J + \pi^2 E_L C_w / L_{z'}^2}{r_2^2} \quad (17)$$

where $L_{z'}$ is the length for twisting about the longitudinal z'-axis. It should be noted that, for the equal-leg angle with different end-restrained conditions, the lengths for bending and twisting may be assumed as the distances between the inflection points of the buckled shapes. Hence, the lengths $L_{x'}, L_{y'}$, and $L_{z'}$ in Eqns. (15) to (17) can be approximated equal to the effective lengths $K_{x'} L_{x'}$, $K_{y'} L_{y'}$, and $K_{z'} L_{z'}$ where $K_{x'}$ and $K_{y'}$ are the effective-length factors about the principal axis x' and y' and $K_{z'}$ is the

warping effective-length factor. It was shown by Trahair (1993) that the values of these factors vary almost linearly with the end restraint parameters from 0.5 for a rigidly restrained end to 1 for an unrestrained end.

The lowest of the solutions P_1, P_2, and P_3 is always less than or equal to the lowest of the buckling loads $P_{x'}$, $P_{y'}$, and $P_{z'}$. By comparing the flexural-torsional buckling loads computed by using Eqns. (14.b) and (14.c), it can be seen that the values of P_3 is always lower than that of P_2. Hence, P_1 and P_3 are the flexural buckling and flexural-torsional buckling equation of the equal-leg angle member, respectively.

Test Specimens, Material Properties, and Test Set-up

The GFRP equal-leg angle members used in this study were made of E-glass fiber-reinforced with polyester resin and manufactured by a pultrusion process. By using the modified ignition loss method (Ye *et al.,* 1995), it was found that the glass fiber volume fraction was about 35% with the filler content about 5 to 10% by volume. Table 1 shows the details of the geometric properties of the GFRP equal-leg angle specimens. The specimen number is designated by a letter "A", leg width, and an identification number. The test consists of 32 specimens with b / t ratios of 8, 12, and 16 and with the slenderness ratios about the minor y'-axis, $L_{y'} / r_{y'}$, ranging from 12 to 187. The $L_{y'} / r_{y'}$ ratios were computed by using the overall length, $L_{y'}$, equals to the actual length of the specimen plus 44 mm due to the height of the test fixture of the supports. Two tests were conducted on each specimen number. The initial crookedness of each specimen was measured prior to the test. It was found that all of the specimens have leg out-of-straightness and leg juncture camber well below the tolerance limit specified by ASTM D3917, which is $L / 240$ and $L / 380$, respectively.

To correlate the analytical results to the obtained test results, the values of σ_L^c, E_L, and G_{LT} are needed to be determined from the compression and in-plane shear coupon test. Nine compression coupons, three coupons from

each angle section, were tested in accordance with ASTM D3410, in order to determine σ_L^c and E_L. All of the compression coupons were prismatic having the width of 38 mm and unsupported coupon lengths of 38, 58, 78 mm for the 6.3, 9.5, and 12.7 mm thick coupon. The coupon lengths were selected to ensure compression failure without buckling of the coupon specimen. Nine shear coupons, three

coupons from each angle section, were also tested in accordance with ASTM D5379, in order to determine G_{LT}. The test is in the form of V-notched beam method under a four-point asymmetric bending configuration. However, the coupons used here (38 by 203 mm) were larger than that given in the standard to reduce material variance associated with nonuniform fiber distributions. This shear test is essentially similar
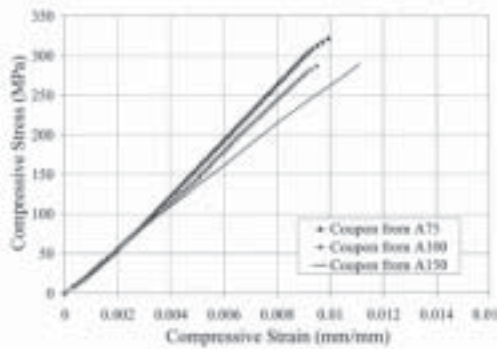

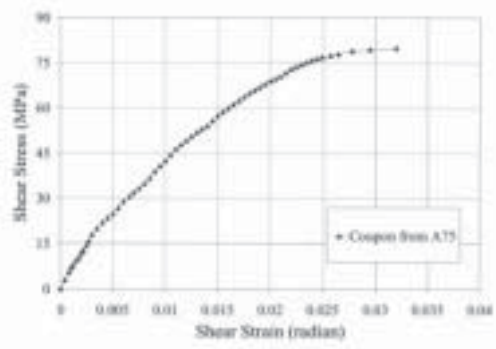Figure 2. Compressive stress-strain curves.

Figure 3. Shear stress-strain curve.

Table 1. Geometric properties of the angle specimens.

Specimen number	Dimension $(b)(t)(L)$ (mm)(mm)(mm)	b/t ratios	Area, A_g (mm²)	$r_{y'}$ (mm)	$L_{y'}/r_{y'}$	Number of specimens
A75-1	(75)(9.5)(305)	8	1,340	14.9	24	2
A75-2	(75)(9.5)(914)	8	1,340	14.9	64	2
A75-3	(75)(9.5)(1,524)	8	1,340	14.9	106	2
A75-4	(75)(9.5)(2,134)	8	1,340	14.9	146	2
A75-5	(75)(9.5)(2,743)	8	1,340	14.9	187	2
A100-1	(100)(6.3)(305)	16	1,241	20.1	17	2
A100-2	(100)(6.3)(607)	16	1,240	20.1	32	2
A100-3	(100)(6.3)(1,524)	16	1,240	20.1	78	2
A100-4	(100)(6.3)(2,134)	16	1,240	20.1	108	2
A100-5	(100)(6.3)(2,743)	16	1,240	20.1	139	2
A150-1	(150)(12.7)(305)	12	3,690	30.1	12	2
A150-2	(150)(12.7)(607)	12	3,690	30.1	22	2
A150-3	(150)(12.7)(914)	12	3,690	30.1	32	2
A150-4	(150)(12.7)(1,524)	12	3,690	30.1	52	2
A150-5	(150)(12.7)(2,743)	12	3,690	30.1	93	2
A150-6	(150)(12.7)(3,660)	12	3,690	30.1	123	2

to that reported by Zureick and Scott (1997). A typical compressive stress-strain curve is shown in Figure 2. Each curve showed a linear elastic response for 85-95% of the ultimate compressive stress. Figure 3 shows a typical shear stress-strain couve. The value for G_{LT} was taken as a chord modulus between 1,000 and 6,000 microstrain. It was found that the average value of σ_L^c, E_L, and G_{LT} are 293.6 MPa, E_L= 28.7 GPa, and G_{LT} = 4 GPa, respectively.

The typical test set-up configuration of the angle specimens is shown in Figure 4. A screw-type testing machine was used to apply the concentric axial load to the angle specimens. The specimen was placed in the testing machine between the pinned-pinned supports. The pinned supports were created using an assenbly of steel plates and hardened steel round bars. Thai cupport configuation permits rotation in two orthogonal directions both about the major x'-axis and the mirror y'-axis. Hence, the terms $K_{x'}$ and $K_{y'}$ in Eqn. (15) and (16) were considered to be 1 To prevent any possible slip or kicking out during loading and to facilitate the alignment of the specimen, the ends of the specimen were held to the stell plate by using four 25 mm-square steel bars which are securely bolted to the steel plate. Due to this end-restrained condition, the term $K_{z'}$ in Eqn. (17) was considered to be 0.5. Before the beginning of the test, a preload of approximately 5 kN was applies to seat the specimen into the testing position. The specimen was tested at a uniform loading rate of 0.5 mm/min and loaded to the point where the specimen was deformed significantly with little or no increase in Load

Results and Discussions

Figure 5 shows typical axial load-displacement curves of the angle specimens. All of the specimens showed a linear elastic response for 80-95% of the buckling load. After reaching the bucking load, the axial displacement increases continuously without any increase in the applied load. There is an exception for the specimen number A150-1 in which the axial load-displacement curves show linear elastic to failure. Both of the angle specimens in this

specimen number were failed by local crushing of the material at an end of the specimens. The stresses at the crushing failure are about twice as low as σ_L^c. By examining the crushing areas, it was found that the failure is due to material defects and/or poor millng at the cutting end of the specimens.

Table 2 shows the experimentally obtained bucking stresses ($\sigma_{\exp}$) and the modes of failure of the angle specimens. Generally, the GFRP

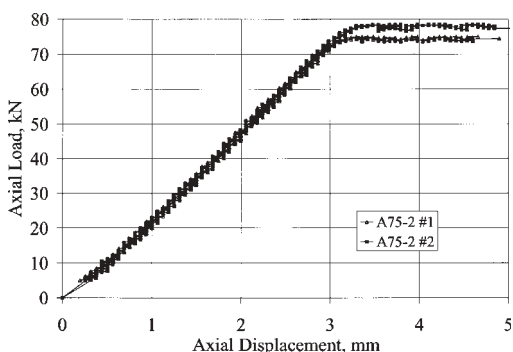**Figure 4. Typical configuration of the test set-up.**

Figure 5. Typical axial load-displacement curves.

angle members buckle in either flexural-torsional buckling or flexural buckling about the minor y'-axis. The flexural-torsional buckling, as shown in Figure 6, was in the form of large lateral deflection about the major x'-axis and twisting of the section about the axis parallel to the longitudinal z'-axis, occurred simultaneously.

The slenderness ratios at which the flexural buckling and the flexural-torsional buckling occur, $(L_{y'}/r_{y'})_{ft/f}$, can be computed by equating P_1 of Eqn. (14.a) to P_3 of Eqn. (14.c). To study the relationship between $(L_{y'}/r_{y'})_{ft/f}$ and b/t ratios, the values of $(L_{y'}/r_{y'})_{ft/f}$ ratio were numerically calculated and plotted for b/t ratios of 8, 12, and 16, and E_L/G_{LT} ratios of 2.6, 5.2, 7.2, 10.4, and 20 as shown in Figure 7. It was found that the relationship is linear similar to that obtained by Zureick and Steffen (2000).

Table 2: Experimentally obtained buckling stresses and modes of failure.

Specimen number	b/t ratios	$L_{y'}/r_{y'}$ ratios	σ_{exp} (MPa)	Ave. σ_{exp} (MPa)	Modes of failure
A75-1	8	24	124.21	120.94	Flexural-torsional buckling
			117.67		Flexural-torsional buckling
A75-2	8	64	77.65	76.12	Flexural-torsional buckling
			74.58		Flexural-torsional buckling
A75-3	8	106	32.50	33.01	Flexural buckling
			33.51		Flexural buckling
A75-4	8	146	16.34	15.71	Flexural buckling
			15.07		Flexural buckling
A75-5	8	187	9.17	9.10	Flexural buckling
			9.02		Flexural buckling
A100-1	16	17	42.30	44.28	Flexural-torsional buckling
			46.26		Flexural-torsional buckling
A100-2	16	32	30.14	28.31	Flexural-torsional buckling
			26.48		Flexural-torsional buckling
A100-3	16	78	25.20	24.07	Flexural-torsional buckling
			22.95		Flexural-torsional buckling
A100-4	16	108	19.49	19.42	Flexural-torsional buckling
			19.35		Flexural-torsional buckling
A100-5	16	139	13.72	13.71	Flexural buckling
			13.70		Flexural buckling
A150-1	12	12	136.70	128.31	Crushing of the material
			119.91		Crushing of the material
A150-2	12	22	68.27	68.42	Flexural-torsional buckling
			68.57		Flexural-torsional buckling
A150-3	12	32	46.08	48.92	Flexural-torsional buckling
			51.75		Flexural-torsional buckling
A150-4	12	52	34.70	37.32	Flexural-torsional buckling
			39.93		Flexural-torsional buckling
A150-5	12	93	32.11	32.54	Flexural-torsional buckling
			32.98		Flexural-torsional buckling
A150-6	12	123	18.70	19.20	Flexural buckling
			19.70		Flexural buckling

By using curve fitting, the relationship is in the form of

$$(18)$$

For the specimens used in this study and having $E_L / G_{LT} = 7.2$, the   ratios for the specimens computed by Eqn. (18) are 82.5, 123.7, and 165 for b / t ratios of 8, 12, and 16, respectively, which is in accordance with the test results. They are about 1.6 times as large as those of structural steel angles having $E_L / G_{LT} = 2.6$. In addition, for a given b / t ratio, the value of   for high orthotropy angle member ($E_L / G_{LT} = 20$) can be 2.7 times as large as that of low orthotropy angle member ($E_L / G_{LT} = 2.6$). It should be noted that the obtained flexural-torsional buckling stresses in the case of low $L_{y'} / r_{y'}$ ratios (i.e., $L_{y'} / r_{y'} < 20$) was significantly less than σ_L^c. This is due to intrinsically high compressive strength-to-modulus ratio of the GFRP material.

Table 3 presents values of the experimentally obtained flexural-torsional buckling stresses along with those predicted (σ_{pred}) by Eqn. (4) and Eqn. (14.c). The $\sigma_{exp} / \sigma_{pred}$ ratios were also presented to show the correlation between the test results and the predicted results. The average $\sigma_{exp} / \sigma_{pred}$ value for the case of Eqn. (14.c) is 1.26 with coefficient of variation (COV) equal to 0.17 and the average value for the case of Eqn. (4) is 1.96 with COV equal to 0.30. It can be seen that the predicted buckling stresses are relatively in good agreement with the test results. Most of the $\sigma_{exp} / \sigma_{pred}$ ratios are larger than 1; this indicates that both equations are conservative. Eqn. (14.c), however, generally predicts the flexural-torsional buckling stresses closer to the test results than Eqn. (4) since Eqn. (4) is a simplified nominal flexural-torsional buckling strength equation (Zureick and Steffen, 2000).

Table 4 presents values of the experimentally obtained flexural buckling stresses along with those predicted by Eqn. (3) and Eqn. (14.a). The average $\sigma_{exp} / \sigma_{pred}$ value for the case of Eqn. (14.a) is 0.96 with COV equal to 0.08 and the average value for the case of Eqn. (3) is 1.15 with COV of 0.24. Therefore,

the test results are quite in good agreement with the predicted results and, in general, Eqn. (14.a) predicts the flexural buckling stresses closer to the test results than Eqn. (3). The lower than predicted experimental buckling stresses is due to many unavoidable factors such as material property variation, load eccentricity, member misalignment, shear effect, and member's out-of-straightness.

Figure 8 presents the plot of the dimensionless ratios of P_1 / P_1 (no shear effect) for a wide range of $L_{y'} / r_{y'}$, for b / t ratios of 8, 12, and 16, and for E_L / G_{LT} ratios of 2.6, 7.2, and 20. By neglecting the transverse shear term from Eqn. (15), Eqn. (14.a) give higher predicted flexural buckling loads in the range of 2.2 to 9.3% with the maximum increasing observed at   . The average value of $\sigma_{exp} / \sigma_{pred}$ in this case is 0.92 with a COV of 0.09. This average value of $\sigma_{exp} / \sigma_{pred}$ is lower than the value that is computed using Eqn. (14.a); indicating that, in general, including the effect of transverse shear into the flexural buckling equations gives a more realistic flexural buckling of the angle member compared to the test results.

Based on the results of this study, the design strength, ϕP_n, for the flexural-torsional buckling and flexural buckling of the equal-leg angle structural members subjected to the concentric axial loads can be taken as the lower of the flexural-torsional buckling and flexural buckling limit state. For a practical angle length, the nominal strength P_n equal to the lower of P_1 and P_3, determined from Eqn. (14.a) and Eqn. (14.c), respectively. Due to the lack of enough testing data for the GFRP materials and the angle members produced by different manufacturers, the target reliability indices for the flexural-torsional buckling and flexural buckling should be at least 3 for the load combination $1.2D + 1.6L$ where D and L are the dead and live loads, respectively. The random variables defining the sectional properties were assumed to be normal distribution and those of the material properties were assumed to be Weibull distribution. Following the component reliability analysis using Monte Carlo simulation, the values of the resistant factor, ϕ, for the flexural-torsional buckling and flexural buckling limit